Title

LIVE-PAINT: Super-Resolution Microscopy Inside Live Cells Using Reversible Peptide-Protein Interactions

Authors

Curran Oi[1,2]

Zoe Gidden[3]

Louise Holyoake[3]

Owen Kantelberg[4]

Simon Mochrie[2,5]

Mathew H. Horrocks*[,4]

Lynne Regan*[,6]

Affiliations

[1]Department of Molecular Biophysics and Biochemistry, Yale University, New Haven, CT 06520

[2]Integrated Graduate Program in Physical and Engineering Biology, Yale University, New Haven, CT 06520

[3]School of Biological Sciences, University of Edinburgh, Edinburgh EH9 3DW

[4]School of Chemistry, The University of Edinburgh, Edinburgh EH9 3FJ

[5]Department of Physics, Yale University, New Haven, CT 06520

[6]Institute of Quantitative Biology, Biochemistry and Biotechnology, Center for Synthetic and Systems Biology, School of Biological Sciences, University of Edinburgh, Edinburgh EH9 3BF

*Correspondence and requests for materials should be addressed to L.R. (email: lynne.regan@ed.ac.uk) MHH (email: mathew.horrocks@ed.ac.uk)

Abstract

We present LIVE-PAINT, a new approach to super-resolution fluorescent imaging inside live cells. In LIVE-PAINT only a short peptide sequence is fused to the protein being studied, unlike conventional super-resolution methods, which rely on directly fusing the biomolecule of interest to a large fluorescent protein, organic fluorophore, or oligonucleotide. LIVE-PAINT works by observing the blinking of localized fluorescence as this peptide is reversibly bound by a protein that is fused to a fluorescent protein. We have demonstrated the effectiveness of LIVE-PAINT by imaging a number of different proteins inside live *S. cerevisiae*. Not only is LIVE-PAINT widely applicable, easily implemented, and the modifications minimally perturbing, but we also anticipate it will extend data acquisition times compared to those previously possible with methods that involve direct fusion to a fluorescent protein.

Keywords

Super-resolution, live cell imaging, fluorescence microscopy, nanobiotechnology, peptide-binding module, coiled coil, peptide, protein, *S. cerevisiae*.

Introduction

Optical microscopy has traditionally been restricted to a resolution of ~250 nm due to the diffraction limit of light. New methods, collectively grouped under the term super-resolution microscopy, have increased the resolution of fluorescence microscopy by almost two orders of magnitude, allowing systems previously inaccessible to fluorescence microscopy to be studied[1-5]. These methods rely on either limiting the illumination of the sample to regions smaller than the diffraction limit[1], or stochastically and temporally separating the emission of individual fluorophores to allow their positions to be precisely localized. This latter strategy is termed single-molecule localization microscopy (SMLM), and various approaches have been developed to enable the required stochastic emission, including stochastic optical reconstruction microscopy (STORM)[5], photo-activation localization microscopy (PALM)[2], and point accumulation for imaging in nanoscale topography (PAINT)[6].

In the original implementation of PAINT, fluorescent molecules (for example, Nile red) bind transiently and non-specifically to hydrophobic regions of a structure[6], and a super-resolution image is built up as each one is localized. Unlike PALM and STORM methods, which are limited by photobleaching of the dye molecules over time, in PAINT-based methods there is continual replenishment of the fluorescent probes, which allows much longer imaging times, resulting in a higher density of localizations, and the potential for a higher resolution image[7]. In all PAINT methods, the concentration of the interacting fluorescent molecule can be varied and optimized.

DNA-PAINT was developed to enable specific and finely tunable binding of the fluorophore to the structure to be imaged[8]. It relies on covalently attaching a short oligonucleotide sequence to the biomolecule of interest. A super-resolution image is built up as fluorescently labeled DNA oligonucleotides, of complementary sequence to the oligonucleotide attached to the biomolecule of interest, transiently hybridize with it and thus are localized. DNA-PAINT is attractive because it is relatively straightforward to vary the strength of strand association by varying the sequence or length of the DNA oligonucleotides. The reversibility of duplex formation allows for replenishment of signal at the position of interest by restricting the illuminated volume of the sample, for example using total internal reflection fluorescence microscopy (TIRFM) or light sheet fluorescence microscopy (LSFM). Thus, only fluorophores in the illuminated portion of the sample are bleached and they will be replaced by unbleached fluorophores when the DNA strands dissociate. By having a large reservoir of fluorophores that can exchange with the bleached ones, many localization events can thus be captured, enabling very high-resolution images to be collected. Localizations with low precision can be discarded, which also contributes to increased resolution.

DNA-PAINT has seen many variations and innovative applications[8-11]. A significant limitation, however, is that DNA-PAINT cannot be used to visualize proteins inside live cells[12]. Although extensions of DNA-PAINT, in which the DNA is fused to a nanobody or another protein-binding module, enable intra-cellular proteins to be visualized, the cell must be permeabilized to allow them to enter. As a result, work in live cells has been

limited to the visualization of cell-surface proteins[12]. Here, we describe a PAINT-based method that has all the advantages of DNA-PAINT, but with the enormous benefit that it can be used for imaging inside live cells. We refer to this approach as LIVE-PAINT (**L**ive cell **I**maging using re**V**ersible int**E**ractions PAINT).

In LIVE-PAINT, reversible peptide-protein interactions, rather than zipping/unzipping of a DNA oligonucleotide duplex, are responsible for the transient localizations required for SMLM. The protein to be imaged is genetically fused to a short peptide and expressed from the protein's endogenous promoter. Additionally, integrated at a suitable place in the genome, a peptide-binding protein is genetically fused to a fluorescent protein (FP) and expressed from an inducible promoter, allowing its expression level to be controlled and optimised. The small size of the peptide tags fused to the protein of interest is another important strength of the method. It enables post-translational fluorescent labeling of target proteins that do not tolerate a direct fusion to a FP. To illustrate this point, we show that LIVE-PAINT can be used to perform *in vivo* super-resolution imaging of proteins, such as actin and cofilin, which are notoriously refractory to direct fusions[13,14]. Furthermore, we show that LIVE-PAINT can be used to perform diffraction-limited tracking of individual biomolecules for extended periods of time.

Results

LIVE-PAINT achieves super-resolution inside live cells using reversible peptide-protein interactions

The essence of LIVE-PAINT is to visualize individual fluorescent molecules transiently attached to a cellular structure of interest. The individual fluorophores are thus identified by temporal, rather than spatial, separation. LIVE-PAINT achieves sparse labeling by using reversible peptide-protein interactions. The protein of interest is directly fused to a peptide and a FP is fused to the cognate protein (Figure 1A). The peptide-protein interactions are chosen so that solution exchange occurs on a timescale shorter than or comparable to the bleaching lifetime, allowing many sequential images to be obtained. In each image, a different peptide-tagged protein of interest is bound to a different protein-FP, allowing individual proteins to be precisely localized (Figure 1A-D). These localization events are then summed to generate a super-resolution image (Figure 1E).

As a test case with which to optimize this approach, we visualized the cell division septin protein Cdc12, a component of the readily-identifiable septum that is formed during *Saccharomyces cerevisiae* budding. We tested LIVE-PAINT using two different peptide-protein interactions with very different dissociation constants and molecular structures: TRAP4-MEEVF (a TPR-peptide pair with a dissociation constant (K_D) of 300 nM) and SYNZIP17-SYNZIP18 (an antiparallel coiled coil pair with a K_D of 1 nM)[15-18]. In both cases, the peptide (MEEVF or SYNZIP18) is fused to Cdc12 and the cognate

protein or peptide (TRAP4 or SYNZIP17, respectively) is fused to the bright green FP mNeonGreen (mNG) (11). Although mNG is known to blink intrinsically[19], we chose to use it in our experiments because it is very bright and therefore can produce very precise localization events. mNeonGreen has a brightness of 93[20], while other FPs we use in this work, mKO and mOrange, have brightness of 31[21] and 49[22], respectively. Most importantly, we show that mKO and mOrange, which are not known to blink intrinsically, are also compatible with LIVE-PAINT (Figure S1 and Supplementary movies 1 and 2). TRAP-peptide pairs have been shown previously to be less perturbative for cellular imaging than direct fusion to a FP[23]. Both TRAP4-MEEVF and SYNZIP17-SYNZIP18, were well-tolerated by the cell, and both can be used for either diffraction limited or super-resolution imaging of the septum in live yeast (Figure 1E). We observed no distorted cell morphology or changes in growth rate in liquid media when using the TRAP4-MEEVF and SYNZIP17-SYNZIP18 interaction pairs. In previous work we observed distorted cell morphology for ~5% of yeast expressing a direct fusion of Cdc12 to an FP[23]. We also provide evidence that LIVE-PAINT can be performed with additional peptide-protein interaction pairs (Figure S2), that the localizations events observed are specific to the protein being labeled (Figure S3), and that two orthogonal interaction pairs can be used with two FPs to tag two different proteins specifically and concurrently (Figure S4).

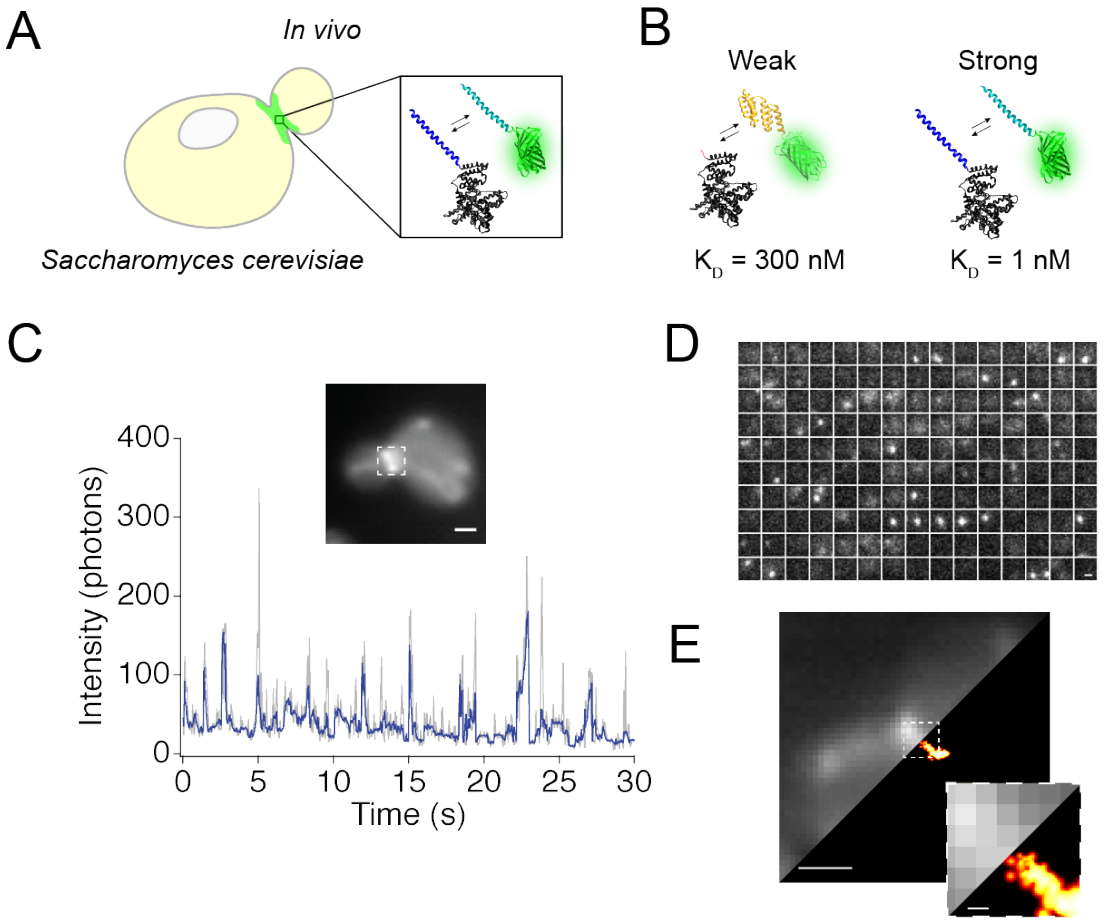

Figure 1. LIVE-PAINT achieves sparse labeling using reversible peptide-protein interactions. (A) Details of the LIVE-PAINT imaging method, as applied to Cdc12. A peptide tag (dark blue) is fused to the target protein that will be imaged, Cdc12 (black). A peptide-binding protein (light blue) is fused to a FP (bright green). The peptide tag and peptide-binding protein reversibly associate, as indicated by the double arrows. (B) Molecular details of the peptide-protein pairs used: TRAP4 (yellow) binds to the peptide MEEVF (red) with a dissociation constant of 300 nM and SYNZIP18 (dark blue) binds to SYNZIP17 (light blue) with a dissociation constant of 1 nM. Proteins are shown with a ribbon representation of their structures, and are approximately to scale. Ribbon structure diagrams were generated using PDB files for interaction pairs similar to those

used in this work: TRAP4-MEEVF is represented using the structure for a tetratricopeptide repeat (TPR) protein in complex with the MEEVF peptide (PDB ID: 3FWV) and SYNZIP17-SYNZIP18 is represented using the structure for the antiparallel coiled coil Kif21A (PDB ID: 5NFD). (C) Binding and unbinding of the peptide-binding module-FP to the peptide tag generate blinking events. Plot of the fluorescence intensity (photons) at a particular location (in a square approximately 1 μm x 1 μm, shown as a dotted box around the septum in the florescence image) in the septum versus time. We interpret these data as peaks in the signal indicating that mNG is bound to Cdc12 and troughs indicating mNG is dissociated from Cdc12. These data correspond to Cdc12 fused to SYNZIP18 being labeled by its interaction with SYNZIP17 fused to the FP mNG. (D) Montage of frames from a fluorescence microscopy video collected of the area of the septum boxed in part (C). Each frame in the montage is separated by 0.2 s and the bright blinking events correspond to fluorescence peaks in (C). (E) Diffraction limited (left) and super-resolution (right) images of the Cdc12 protein imaged using Cdc12-SYNZIP18 and SYNZIP17-mNG. Number of super-resolution localization events: 448. Scale bars are 1 μm, except for the inset to (E), which has a 100 nm scale bar.

Low FP expression levels result in a higher percentage of bona fide localization at the septum

In LIVE-PAINT, the peptide-binding proteins fused to mNG (TRAP4-mNG and SYNZIP17-mNG), are expressed from an inducible promoter, so that expression levels can be optimized[24]. See Figure S5 for fluorescence induction profile.

By varying the expression level of either TRAP4-mNG or SYNZIP17-mNG, for the TRAP4-MEEVF and SYNZIP17-SYNZIP18 interaction pairs respectively, we can determine which conditions generate the highest percentage of localizations at the septum relative to non-specific localizations (Figure 2). For very low expression levels, for example for 0% galactose with 'leaky' expression, not enough mNG is expressed and not enough localization events are achieved to generate a super-resolution image. Conversely, for example for 0.1% galactose, expression levels are too high and very few individual localization events can be visualized, because the density of mNG is too high to achieve sparse labeling. At intermediate expression levels, for example with 0.005% or 0.02% galactose, there are sufficient FPs that enough localization events can be recorded to resolve a super-resolution image, but the FP expression level is not so high that single localization events cannot be recorded.

We performed cluster analysis using the DBSCAN function (see methods) to quantify the number of localization events in the septum versus in the rest of the cell. We were thus able to identify the conditions that produced the most specific super-resolution

images. In an analogous fashion to DNA-PAINT, the FP mNG does not give rise to a localization event until it binds and is immobilized. Some non-specific localization or blinking events are recorded, these are randomly distributed within the cell and can be removed from further analysis by using DBSCAN. The number of these non-specific localization events increases with galactose concentration, because by increasing galactose we increase the number of free mNG which are not bound to a Cdc12 protein. For this reason, we choose not to work with very high galactose concentrations for most of our experiments. We observed that the highest percentage of localization events in the septum for the 0.005% galactose condition when imaging both the TRAP4-MEEVF interaction pair (45% of localization events in the septum) and the SYNZIP17-SYNZIP18 interaction pair (98% of localization events in the septum). The septum was identified by cluster analysis (see methods).

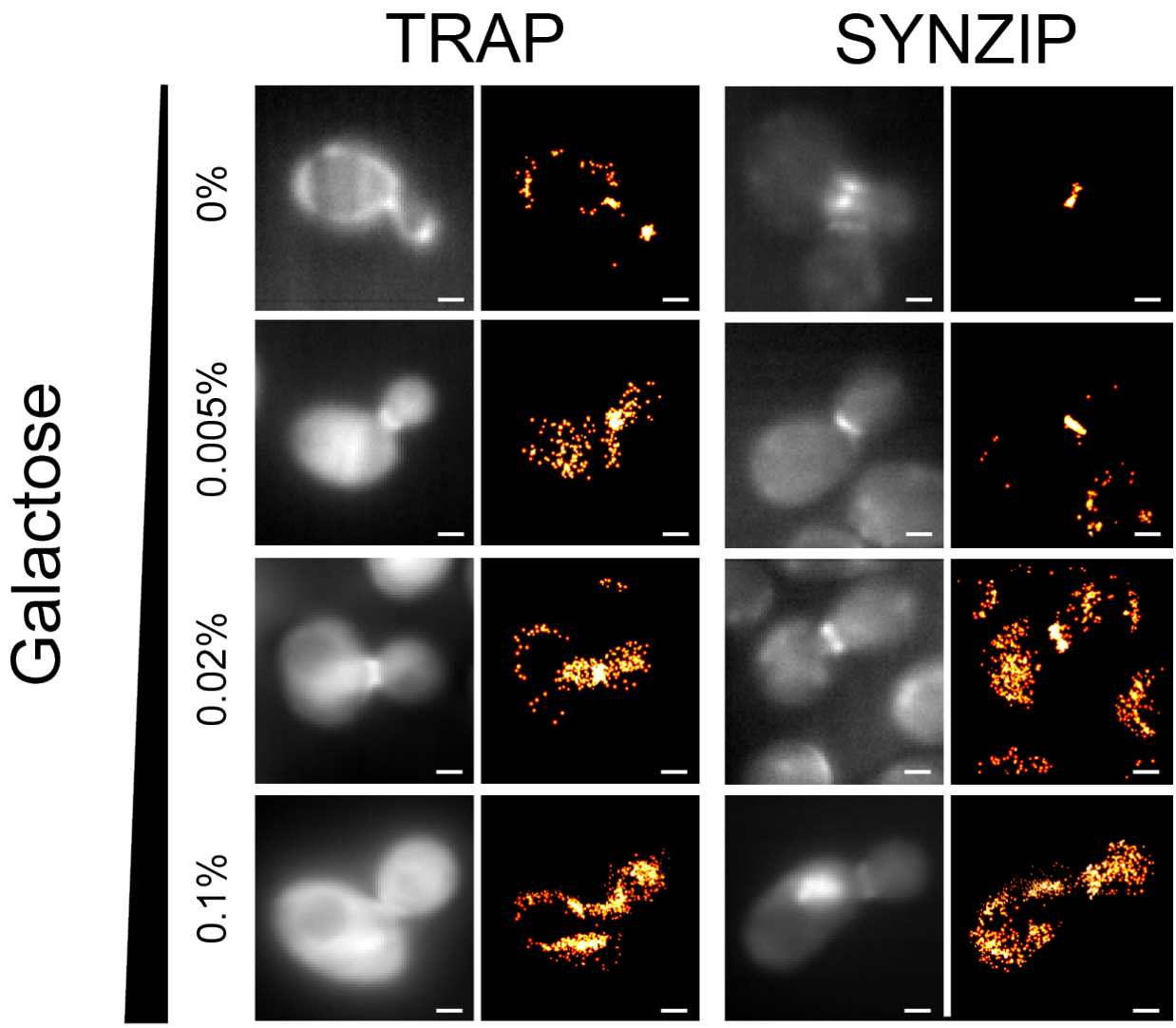

Figure 2. Varying either the FP expression level or the peptide-protein interaction pairs changes the number of localization events, which are specifically localized to the yeast bud neck during cell division. Pairs of diffraction-limited and super-resolution images are shown for Cdc12-MEEVF + TRAP4-mNG (left) and Cdc12-SYNZIP18 + SYNZIP17-mNG (right), at different concentrations of galactose (as indicated on the left). Percent of localizations in septum, at different concentrations of galactose, for Cdc12-MEEVF + TRAP4-mNG: 0% galactose - 15%; 0.005% galactose - 45%; 0.02% galactose - 38%; 0.1% galactose - 23%. Percent of localizations in septum, at different

concentrations of galactose, for Cdc12-SYNZIP18 + SYNZIP17-mNG: 0% galactose - 94%; 0.005% galactose - 98%; 0.02% galactose - 43%; 0.1% galactose -19%. See Table S1 for total number of localizations per image. Scale bars are 1 μm.

Septum width increases with increasing yeast daughter:mother diameter ratio

To demonstrate the potential of LIVE-PAINT, we show an example of how it can be used to study a biological structure in live cells. By analyzing SMLM data for Cdc12 in individual cells, obtained using LIVE-PAINT with the SYNZIP17-SYNZIP18 interaction pair, we are able to describe various features of the yeast budding process. For example, we find that for small daughter cell sizes (daughter:mother diameter ratio less than approximately 0.85), the septum width is of the order 200 nm. As the daughter cell gets larger (daughter:mother diameter ratio approximately 0.85 to 1.0), the septum is clearly visible as two separate rings, with a septum width of approximately 400-800 nm. See Figure S6. This example demonstrates that LIVE-PAINT can be used to study a biological structure in live cells on the single cell level.

Labeling using a construct with three tandem copies of mNG improves localization precision compared to a single copy.

In current super-resolution imaging techniques used inside live cells, such as PALM, the target protein is directly fused to a FP. This fusion adds a large, 25 kDa, modification to the target protein. Trying to enhance the PALM signal by fusing three FPs to the same target protein, would increase the size of the overall protein by about 75 kDa. Many proteins are unable to fold and correctly mature to their functional state when fused to a single FP, therefore a larger modification to a target protein, on the order of 75 kDa would likely be even more detrimental.

With the LIVE-PAINT method, however, the protein of interest is labeled post-translationally and reversibly. Thus, labeling with multiple tandem FPs should be more feasible. We performed LIVE-PAINT on Cdc12-SYNZIP18 using the SYNZIP17 fused to one or three tandem copies of mNG and compared the super-resolution data obtained for both conditions (Figures S7 and S8). Cdc12 not only tolerates such post-translational labeling with the three tandem mNG, but labeling with this construct results in better localization precision. We note, however, that the larger size of the three tandem mNG construct creates additional distance between the protein of interest which would result in increased uncertainty about its actual position.

LIVE-PAINT enables longer data acquisition times

An additional advantageous feature of the LIVE-PAINT method is that it allows bleached fluorescent labels to exchange with unbleached fluorescent labels, *in vivo*. In the case of STORM and PALM imaging methods, photobleaching of the probe adds a limitation to the number of emitters that can be localized. This photobleaching reduces the resolution of the image because it limits the density of emitters that can be measured. Thus, researchers have to resort to using localization events with lower signal to noise than is optimal. In many cases, control of the emission is difficult to achieve, and much of the fluorescent probe is bleached early in the acquisition when individual emitters cannot be discerned due to their density being too high, further limiting the density of localizations measured. Here we demonstrate the ability to image for longer periods of time with LIVE-PAINT, using the SYNZIP labeling pair.

When imaging using a conventional direct fusion of Cdc12 to mNG, we observe that after we deliberately photobleach by irradiating with high laser power for two minutes, very few localization events are subsequently observed. In contrast, when using SYNZIP17-SYNZIP18 to localize mNG to Cdc12, after we deliberately photobleach by irradiating with high laser power for two minutes, we subsequently observe many more new localization events, indicating that the bleached SYNZIP17-mNGs can unbind and be replaced by unbleached SYNZIP17-mNGs from the cytoplasm. This result shows that the LIVE-PAINT imaging strategy allows one to obtain more total localization events during an imaging session, because they allow for longer imaging times (Figure 3). The

individual cells imaged using LIVE-PAINT for the data in Figure 3 were measured to have a resolution of ~20 nm (see Figure S9 for maximum projection images of the individual cells analyzed in Figure 3).

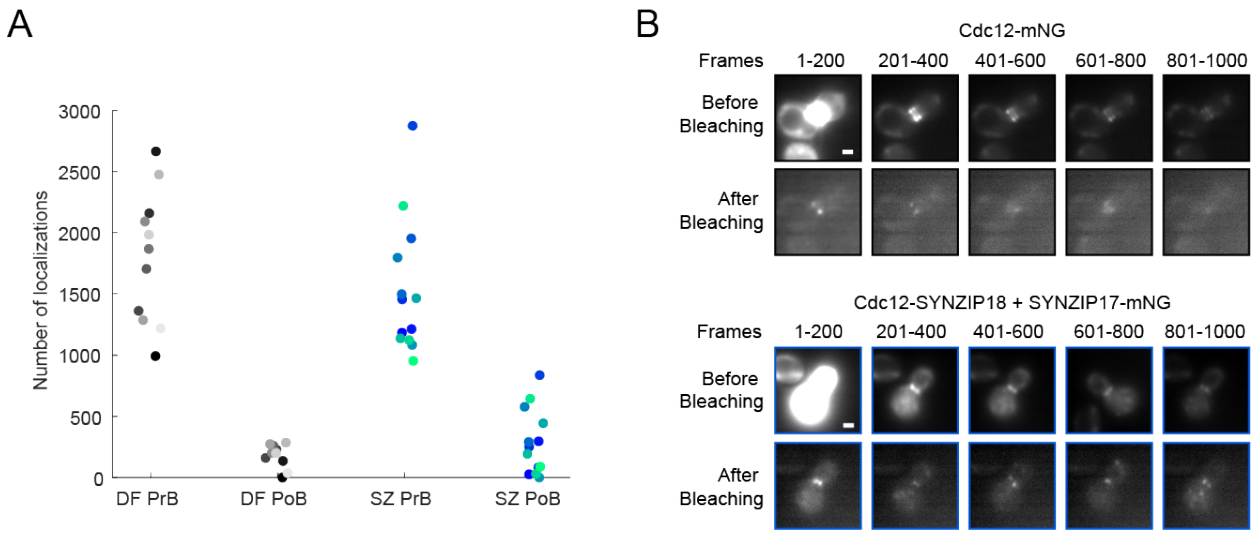

Figure 3. LIVE-PAINT shows recovery of signal after bleaching. (A) LIVE-PAINT interaction pairs show more recovery in number of localization events than a direct fusion to a FP. In this experiment, fluorescence images were collected for 1,000 frames (50 s) at standard imaging power (3.1 W/cm^2), then the sample was photobleached using high laser power (26.6 W/cm^2), and then the sample was again imaged for 1,000 frames (50 s) at standard imaging power. Cdc12-SYNZIP18 + SYNZIP17-mNG (blue/green circles, each representing a single cell) retain many more localization events than Cdc12-mNG (gray circles, each representing a single cell) after two minutes of photobleaching. Each shade of gray or blue/green represents a single cell, which can be color-matched between pre-photobleaching (PrB) and post-photobleaching (PoB) conditions. DF = Cdc12-mNG (Direct Fusion); SZ = Cdc12-SYNZIP18 + SYNZIP17-mNG (SYNZIP pair). (B) Maximum projections for different frame ranges in both “before bleaching” and “after bleaching” videos demonstrate that signal obtained after bleaching continues to localize to the yeast septum. (Top) Maximum projections are shown for 200 frame ranges for a representative cell expressing Cdc12-mNG. (Bottom) Maximum projections are shown for a representative cell expressing Cdc12-SYNZIP18 +

SYNZIP17-mNG. All “before bleaching” images are normalized to one another and, similarly, all “after bleaching” images are normalized to one another. Scale bar is 1 μm.

LIVE-PAINT signal replenishment increases with increasing concentration of FP

The data in Figure 3 shows that reversible interaction pairs can unbind from the target protein and signal can be replenished by free protein-mNG binding to the target protein.

Building on this result, we compared how long data collection can be continued, when there is a high versus low level of peptide-binding protein-mNG in the cytoplasm. Figure 4 shows the results of such experiments for both the SYNZIP17-SYNZIP18 and TRAP4-MEEVF interaction pairs. For 0% galactose, where the expression level of peptide-binding-module-FP is low, almost all the binding-module-FP will be initially bound to Cdc12, thus all FPs will be illuminated and bleached rapidly, because there is not a cytoplasmic pool of peptide-binding-protein-FP for them to exchange with. By contrast, for 0.1% galactose, where the expression level of the peptide-binding protein-FP is high, there is a sizeable cytoplasmic pool available to exchange with molecules bound to peptide-Cdc12, but which have been bleached. In Figure 4B, for example, we observe that when imaging Cdc12-SYNZIP18 + SYNZIP17-mNG using 0.1% galactose, even after 200 s of imaging, localizations are still being recorded at about 30-40% of the initial rate.

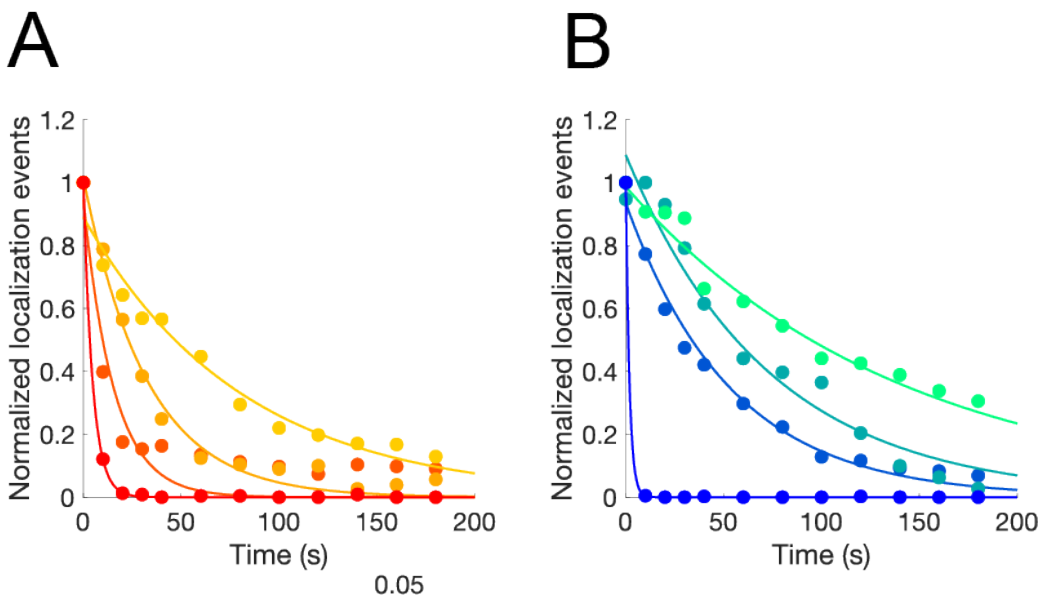

Figure 4. Localization rate decays more slowly with increased FP expression. Localization rate as a function of imaging time for (A) Cdc12-MEEVF + TRAP4-mNG and (B) Cdc12-SYNZIP18 + SYNZIP17-mNG, each at four different concentrations of galactose. Data for the MEEVF-TRAP4 interaction pair is for 0% galactose (red), 0.005% galactose (dark orange), 0.02% galactose (light orange) and 0.1% galactose (yellow). Data for the SYNZIP18-SYNZIP17 interaction pair is for 0% galactose (bright blue), 0.005% galactose (blue), 0.02% galactose (teal) and 0.1% galactose (mint). The data for each concentration of galactose were fit to a single exponential (shown as a solid line with matching color). For the MEEVF-TRAP4 interaction pair (A), the exponential time constant (τ) for the different concentrations of galactose is 0%: 4.7 s; 0.005%: 15 s; 0.02%: 32 s; 0.1%: 81 s. For the SYNZIP18-SYNZIP17 interaction pair (B), the exponential time constant (τ) for the different concentrations of galactose is: 0%: 1.9 s; 0.005%: 54 s; 0.02%: 73 s; 0.1%: 139 s.

LIVE-PAINT can be used to image proteins that are refractory to direct fusion to a large protein

Actin, an important cytoskeletal protein, is notoriously difficult to tag and image. A number of different methods have been developed to circumvent this problem, but they are not without issues, including changing the stability, dynamics, and lifetime of actin structures[13,25,26]. Moreover, very few of these methods can be used inside live cells and none is currently compatible with live cell super-resolution imaging. We therefore investigated if LIVE-PAINT could be used to image actin. Wild-type actin was chromosomally expressed from its endogenous promoter. We expressed SYNZIP18-actin from a low copy number plasmid, using a copper-inducible promoter. SYNZIP17-mNG was expressed, as previously, from the galactose inducible promoter, chromosomally integrated at the GAL2 locus (Figure 5).

Using LIVE-PAINT, we were able to readily visualize actin patches, which assemble at the cell membrane, at sites of endocytosis[27] (Figure 5A). Because actin structures are quite dynamic, we investigated how quickly we could obtain super-resolution images (compared to the acquisition time of 200 s for the data shown in Fig 5C). Actin rings, or actin cables that span the cell, are likely not observed because we are imaging in TIRF, which illuminates only about 200 nm into the cell (a typical yeast cell is 1-3 μm thick). Alternatively, or additionally, it could be that the stringent structural requirements for actin in these assemblies means that even actin with very small ~2 kDa tags may be

excluded from ring and cable structures[28]. We find that with a data acquisition time as short as 3 s, we can obtain data with a resolution of approximately 50 nm (Figure S10).

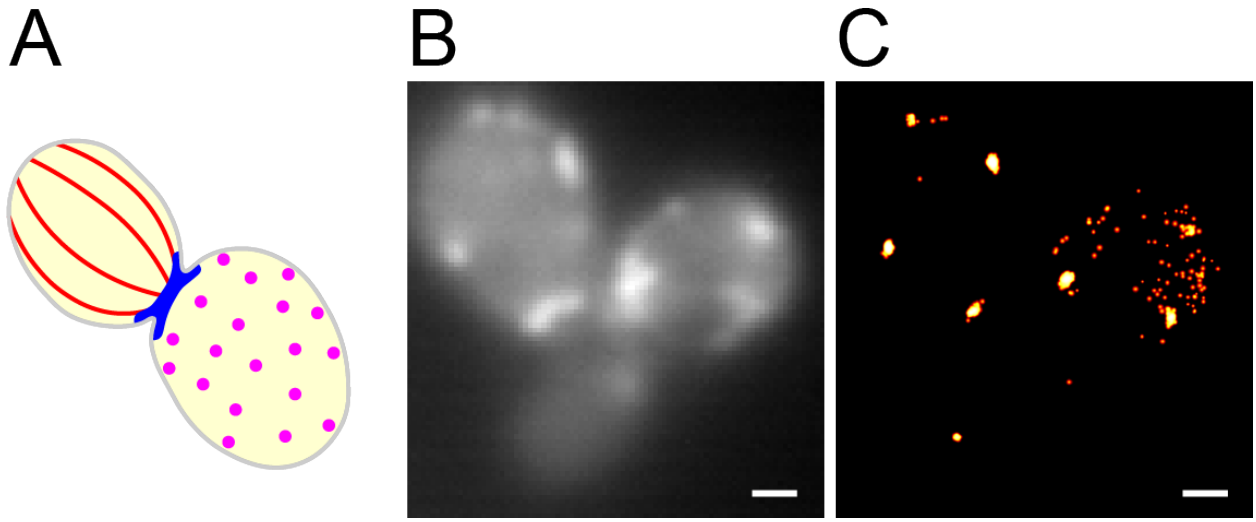

Figure 5. Actin patches can be imaged using LIVE-PAINT in live yeast. (A) Cartoon showing the three distinctive actin structures that have been observed in fixed and immunostained *S cerevisiae*: actin cables (red), actin rings (blue), and actin patches (magenta). (B) Diffraction limited image of SYNZIP18-actin + SYNZIP17-mNG. (C) LIVE-PAINT super-resolution image constructed from 200 s video imaging SYNZIP18-actin + SYNZIP17-mNG. Number of localization events obtained: 778. Only localization events with precision < 30 nm were used to construct the super-resolution image. Scale bars are 1 μm.

LIVE-PAINT enables long tracking times *in vivo*

In the data presented so far, we have used LIVE-PAINT to generate super-resolution images of proteins which do not move significantly during the period of data acquisition. The extended imaging lifetime enabled by LIVE-PAINT, however, offers the opportunity to detect and track the motion of diffusing molecules within live cells. Cofilin is an important protein that binds to actin filaments promoting severing[14]. It has so far, however, proven difficult to image due to its function being affected by either N- or C-terminal direct fusion of an FP[14]. We therefore C-terminally tagged cofilin with SYNZIP18, and tracked it using the LIVE-PAINT strategy (diffraction-limited, not super-resolution). We were able to observe the diffusion of cofilin during the 100 s of imaging (Figure 6 and Supplementary Movie 3). We observed a wide range of behaviors (Figure 6).

The success of the LIVE-PAINT tagging approach in these examples demonstrates the value of the method for visualizing proteins that are refractory to direct fusion to an FP[14], and also its potential to be developed to track moving proteins.

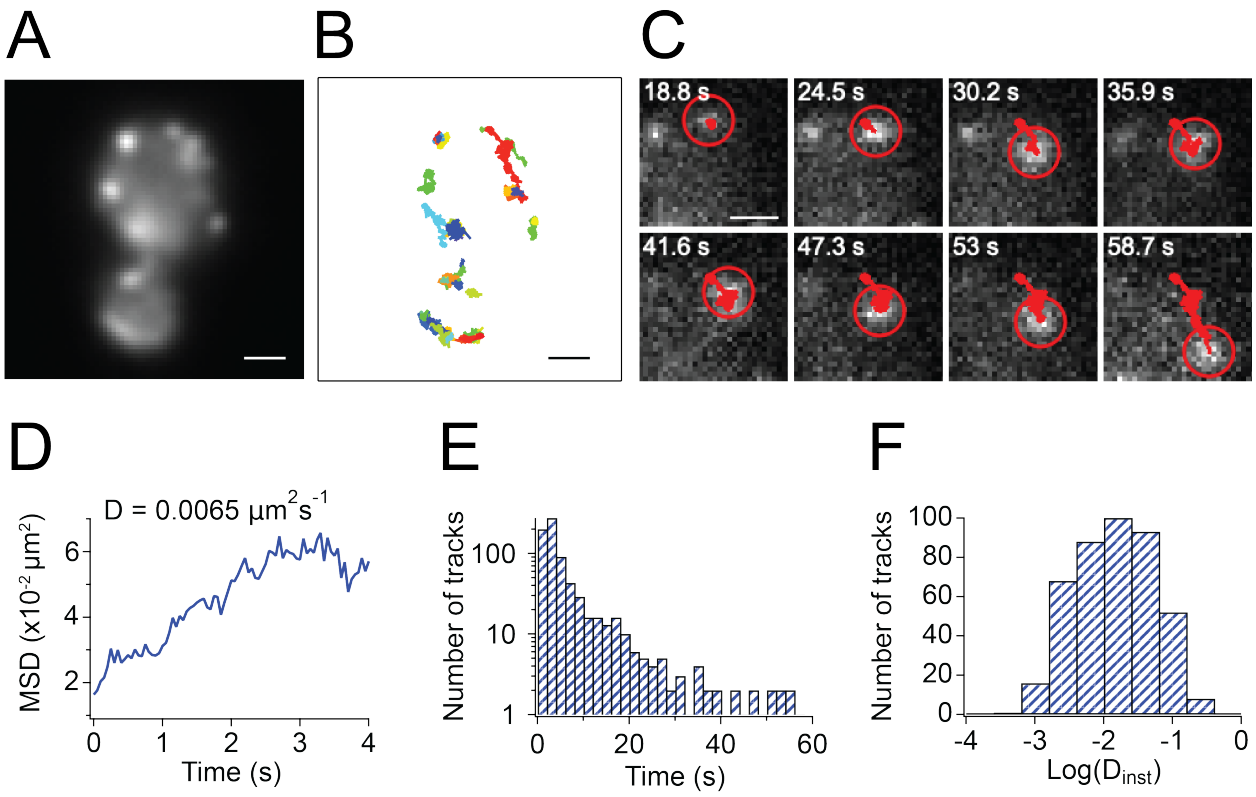

Figure 6. Clusters of cofilin can be tracked using LIVE-PAINT. (A) Diffraction-limited image of example live yeast in which cofilin was tagged and tracked. Larger field of view shown in Figure S11. (B) Individual tracks of cofilin from the cells shown in (A). The yeast cells were imaged for 100 s, and each colored track corresponds to an individual diffusing cluster (see Supplementary Movie 3). (C) Example montage of one of the diffusing cofilin clusters (see Supplementary Movie 4). (D) The mean squared displacement of the tracked cofilin cluster shown in (C). (E) Histogram of track lengths from all clusters detected in the cells in Figure S11. The tracks last for 6.59 ± 9.83 s (mean ± S.D., n = 426). (F) Histogram of the diffusion coefficients of the tracked cofilin clusters. D = 0.031 ± 0.043 $\mu m^2 s^{-1}$ (mean ± S.D., n = 426). Scale bars are 1 μm.

Discussion

We have developed an imaging strategy, LIVE-PAINT, which enables a new approach to super-resolution imaging inside live cells. We have demonstrated the effectiveness of LIVE-PAINT, which makes use of reversible protein-peptide interactions to obtain SMLM in live *S. cerevisiae*. The data we obtained for Cdc12 enabled us, for example, to quantitatively track the width of the septum at the bud neck of budding yeast as a function of daughter:mother cell diameter ratio and showed that septum width does not change significantly until the daughter diameter reaches approximately 0.85 of the mother cell diameter, at which point the septum divides into two distinct rings.

LIVE-PAINT has a number of advantages over existing super-resolution imaging methods. The main advantage over DNA-PAINT is that LIVE-PAINT works inside living cells; all the components that we describe are chosen to function in that *milieu*. Also, LIVE-PAINT is extendible to concurrent tagging of multiple protein targets (Figures S1-S4). Recently, interacting charged coiled coil pairs have been used to label proteins to perform PALM imaging in live mammalian cells[29]. This work provides a valuable independent validation of our approach.

LIVE-PAINT requires neither photo-conversion of fluorophores (as PALM does) nor selective deactivation of fluorophores as stimulated emission depletion (STED) does. Not only do these methods require special instrumentation, but the high laser power that is typically required can often cause cell damage during live cell imaging experiments, in

addition to bleaching of fluorophores[30]. LIVE-PAINT is performed inside living cells, typically in minimal growth medium, with no potentially toxic additions, such as oxygen scavengers, required. LIVE-PAINT requires only that the protein of interest is directly fused to a small peptide tag, a strategy with a number of advantages. Labeling is post-translational, and therefore the method is suitable for labeling proteins for which direct fusion to a larger FP abrogates function[23]. Other approaches to performing PAINT in live cells, such as protein-PAINT, require the addition of organic dyes, cannot be used to image multiple targets simultaneously, and require a larger fusion to the target protein[31].

The intensity of the signal from each localization event can be increased, by using a tandem array of FPs attached to the peptide-binding protein. It is also straightforward to change the identity of the FP, without needing to change the peptide fusion to the protein to be imaged. Because LIVE-PAINT does not rely on the use of photoactivatable proteins, any FP can be used. This flexibility in choice of FP means that the method could be extended to concurrent super-resolution imaging of multiple targets. One of the limitations of existing live cell super-resolution methods is the reliance on FPs that are all very spectrally similar to one another, which prevents accurate imaging of multiple target proteins concurrently. Even though recent methods have been extended to image two targets in live cells, they require harsh oxygen scavengers and are limited to only two colors by the lack of additional orthogonal chemistries for attachment of dyes to protein tags such as SNAP-tag[32]. LIVE-PAINT does not require oxygen scavengers and

is limited only by the number of orthogonal peptide-protein interaction pairs and the number of available spectrally distinct FPs, both of which are abundant.

Importantly, the protein of interest is expressed from its endogenous promoter and the conditions for detection of fluorescence localizations are optimized by adjusting the intracellular concentration of the peptide-binding protein-FP that is used for labeling. This means that for a very abundant protein of interest, for example, in LIVE-PAINT the number of FPs can be reduced by reducing the expression level of the peptide-binding protein-FP, instead of having to photobleach some of the FPs to reduce the number so that individual FPs can be localized. Similarly, for a low abundance protein of interest directly fused to an FP, photobleaching is especially problematic, because the starting number of molecules is very low. In LIVE-PAINT, more localization events can be observed by imaging for longer, during which time any bleached peptide-binding protein-FPs can be refreshed by exchange with an unbleached pool.

Finally, LIVE-PAINT, especially in a TIRFM (or LSFM) format, enables data to be acquired for much longer than other current methods (such as PALM) that can be used inside live cells. In such methods, the FP is directly fused to the protein of interest, so once a fluorophore is bleached, it is not replaced and from then onwards is dark. By contrast, in LIVE-PAINT, the non-covalently bound FP can be exchanged after bleaching, with a non-bleached FP from the cytoplasm. Acquiring data for longer results in more localizations being detected and consequently higher resolution images being obtained. Unbound FPs in LIVE-PAINT result in background fluorescence, but this

effect can be mitigated by reducing the illumination volume in the cell, as we have done using TIRFM in this work, or by using other strategies, such as light-sheet fluorescence microscopy (LSFM).

We have demonstrated the power of LIVE-PAINT in *S. cerevisiae* by using it to image Cdc12 and hence to study septum formation. Furthermore, we have used it to image actin and cofilin, two important proteins that are intractable to direct fusion. Finally, we showed that this approach is fundamentally compatible with tracking the movement of individual proteins inside live cells.

We expect that it will be straightforward to extend LIVE-PAINT to other organisms and cell types. In our work we found that two of the three peptide-pairs that we tested were suitable for LIVE-PAINT. Many more potentially compatible interaction pairs exist, and may be better suited for particular applications. In future work, we will investigate how the optimal labeling requirements differ for different cellular proteins and how best to label and image multiple proteins simultaneously.

Methods

Molecular biology

All cloning was performed in *Escherichia coli* strain TOP10. Peptide tags were cloned into pFA6a-KANMX6 by amplifying the plasmid backbone and inserting gBlocks (Integrated DNA Technologies) using NEBuilder® HiFi DNA Assembly Master Mix (New England Biolabs). Except where otherwise noted, the protein sequence used to link different protein components was GGSGSGLQ. The two residue linker, GS, was used between the mNG proteins to create the three mNG array. The 3xmNG construct itself was joined to SYNZIP17 using our standard GGSGSGLQ linker.

Peptide-binding proteins fused to FPs were cloned into the pFA6a-HIS3MX6 and tagged actin constructs were cloned into the pCu415CUP1 vector (CEN6/ARS4 origin of replication) using the methods referenced above.

The linker used to fuse actin to SYNZIP18 or MEEVF was GGSGSG.

Primer sequences used in this study are listed in Tables S3, S4, and S5.

Peptide-protein interaction selection

TRAP4-MEEVF[15], SYNZIP17-SYNZIP18[17], and CC-$A_N^{3.5}$-CC-$B_N^{3.5}$ [33] interaction pairs were identified in the literature and tested *in vivo* in live yeast by fusing one half of the interaction pair to a protein of interest and the other half to a FP. The cells were imaged under a microscope as described in the “Microscopy” section. The TRAP4-MEEVF and SYNZIP17-SYNZIP18 interaction pairs showed no morphological abnormalities, no noticeable growth defect in liquid culture or on plates and showed fluorescence at the

expected locus of the tagged protein. For this reason, these two interaction pairs were used in this work. Using CC-$A_N^{3.5}$-CC-$B_N^{3.5}$ interaction pair resulted in unusual cell morphology in the vast majority of cells, with elongated cell shapes, so this pair was not used further. The 101A-101B and 108A-108B interaction pairs[18] were also checked and did not cause any changes to cell morphology or changes to cell growth.

Yeast strain construction

Except where otherwise noted, standard methods for genetically modifying yeast and preparing growth media were used[34]. The yeast strains and selection markers used in this study are listed in Table S2.

Yeast strains constructed in this study are all derived from the parent strain BY4741.

C-terminal tags were amplified from pFA6a-kanMX6 yeast integration vectors, along with the KanR marker. The amplification primers also included 45 bp homology arms, which matched the final 45 bp preceding the stop codon in the protein to be tagged and 45 bp downstream of the stop codon.

Transformants were selected by plating first on YPD plates and then replica plating to yeast agar plates including 600 mg/L geneticin (Gibco) and incubating for a further 16 hours.

FP fusions were inserted into the yeast genome at the GAL2 locus by amplifying the desired protein's sequence from a plasmid. The amplification primers also included 45 bp homology arms that match sequences upstream and downstream of the GAL2 gene, and the HIS3 gene.

Transformants were selected by plating on synthetic complete agar plates lacking histidine.

Strain construction was verified by PCR amplification of the modified locus (using primers from Table S3).

First, genomic DNA (gDNA) was isolated from colonies obtained from yeast transformations. This was done by resuspending a single yeast colony in 100 µL of 0.2 M LiAc + 1% SDS. This mixture was incubated at 75°C in a heat block for 5 minutes. Afterwards, 300 µL 100% ethanol was added to the mixture and centrifuged at 15,000 xg for 3 minutes. The resulting pellet was washed with 100 µL 70% ethanol, the ethanol was removed, and the pellet allowed to dry for 10 minutes. The dried pellet was then dissolved in 20 µL TE buffer (10 mM Tris pH 8.0, 1 mM EDTA pH 8.0) and centrifuged at 15,000 xg for 15 seconds. The supernatant containing the gDNA was then transferred to a fresh tube.

This gDNA was then used as a template for a PCR reaction to confirm the presence of the inserted DNA at the genomic locus being checked. The PCR reactions were carried

out using Phusion High-Fidelity DNA Polymerase and GC buffer (New England Biolabs) in a ProFlex PCR system (Thermo Fisher Scientific). All PCR reactions to validate the insertion of DNA at genomic loci ran for 30 cycles and used an extension time of 2 minutes and a volume of 10 μL. The annealing temperatures used for checking each locus varied: CDC12 (59°C), GAL2 (64°C), and COF1 (61°C). PCR products were run on a 1% agarose gel in TAE buffer (40 mM Tris, 20 mM acetic acid, and 1 mM EDTA pH 8.0) for 30 minutes at 120 V.

Microscopy

For imaging experiments, yeast cells were grown overnight in 500 μL of synthetic complete media. Constructs using the galactose inducible promoter, pGAL1, were all grown with 1% w/v raffinose plus the concentration of galactose desired for a particular experiment. The concentration of galactose used varied between 0% and 2% w/v.

One colony was picked into a 500 μL overnight culture to ensure that the OD_{600} of the cells was between 0.1 and 0.5 by the time of imaging. Two dilutions of the overnight culture, 1:1 and 1:5, were prepared to ensure that one would fall in this OD_{600} range.

22x22 mm glass coverslips with thickness no. 1 (VWR) were cleaned by a 20 minute exposure in a 2.6 L Zepto plasma laboratory unit (Diener Electronic). Frame-Seal slide chambers (9 × 9 mm^2, Biorad, Hercules, CA) were then secured to a coverslip. The surface was prepared for the attachment of yeast cells by coating the surface with 2 mg/mL concanavalin A (Sigma-Aldrich), which was dissolved in PBS pH 7.4, using

approximately 100 μL per well. After leaving the concanavalin A on the surface of the slide for 30 seconds, it was removed using a pipette tip and by tilting the slide to ensure all liquid was removed. Then, 150 μL of prepared yeast culture was pipetted onto the slide. The yeast culture was left to sit on the slide for approximately 5 minutes. The cells were then aspirated from the slide, the surface washed with milliQ water three times, and then 150 μL fresh milliQ water was then added to the slide before imaging.

Single-molecule imaging was performed using a custom-built TIRF microscope, which restricts the illumination to within 200 nm of the sample slide. The fluorophores were excited with 488 nm illumination. Collimated laser light at a wavelength of 488 nm (Cobolt MLD 488-200 Diode Laser System, Cobalt, Sweden) was aligned and directed parallel to the optical axis at the edge of a 1.49 NA TIRF objective (CFI Apochromat TIRF 60XC Oil, Nikon, Japan), mounted on an inverted Nikon TI2 microscope (Nikon, Japan). The microscope was fitted with a perfect focus system to autocorrect the *z*-stage drift during imaging. Fluorescence collected by the same objective was separated from the returning TIR beam by a dichroic mirror (Di01-R405/488/561/635 (Semrock, Rochester, NY, USA), and was passed through appropriate filters (BLP01-488R, FF01-520/44 (Semrock, NY, USA)). The fluorescence was then passed through a 2.5× beam expander and recorded on an EMCCD camera (Delta Evolve 512, Photometrics, Tucson, AZ, USA) operating in frame transfer mode (EMGain = 11.5 e^{-}/ADU and 250 ADU/photon). Each pixel was 103 nm in length. Images were recorded with an exposure time of 50 ms with a laser power density of 3.1 W/cm^2. The lasers were first attenuated with neutral density filters to reduce the excitation power. The power at the

back aperture of the objective lens was measured, and the excitation area determined using tetraspeck beads immobilized on a glass coverslip. The microscope was automated using the open source microscopy platform Micromanager.

For photobleach-and-recovery experiments we first imaged the samples at very high laser power density (26.6 W/cm^2). After 1,000 frames (50 s) of imaging, this power density was dropped to 3.1 W/cm^2. The sample was then imaged for another 1,000 frames (50 s).

Microscope settings/Imaging parameters

Images were analyzed using Fiji and single localizations were processed using the Peak Fit function of the Fiji GDSC SMLM plugin, using a signal strength threshold of 30, a minimum photon threshold of 100, and a precision threshold of 20 nm. The precision threshold was sometimes changed to 30 nm, 40 nm, or 1000 nm, in order to obtain the distribution of precision values for all obtained localization events. Figure S12 shows a matrix of precision and minimum photons per localization thresholds applied to one stack of images, which helped select the cutoffs used.

Image resolution calculation

Image resolution was calculated by first performing cluster analysis using DBSCAN[35] in Python 2.7 to identify localizations in the yeast bud neck. Then, resolution was measured using the equation $R_{eff} = \sqrt{(\bar{r}_{nn})^2 + (\bar{\sigma})^2}$, where R_{eff} is the effective image

resolution, $\bar{r}_{nn}$ is the mean nearest neighbor distance between localizations in the septum, and $\bar{\sigma}$ is the average localization precision[36].

Cluster analysis for identifying yeast septum

For the images shown in Figure 2, septum localizations were identified from total cellular localization events using DBSCAN[35] in Python 2.7 and the percent of total cellular localizations in the septum was determined. In order to prevent misidentification of septa in background localizations, DBSCAN was applied to localizations within a 1 μm radius of the center of the cell. DBSCAN parameters were maintained for images of cells the same galactose concentration: 0% galactose - ε = 2, N = 25; 0.005% galactose - ε = 2, N = 50; 0.02% galactose - ε = 1.75, N = 50; 0.1% galactose - ε = 2.8, N = 75.

Quantifying septum width

Budding yeast with septa were identified from z-projections and following thresholding, ImageJ's Analyze Particles tool was used to determine: the maximum Feret's diameter of the cell, the starting coordinates of the Feret's diameter, the angle between the Feret's diameter and the x-axis, and the coordinates of the cellular center of mass. The end coordinates of the Feret's diameter were calculated from the Feret's diameter data. In the same cells, septum localizations were identified from total cellular localization events as described in above cluster analysis within a radius of the Feret's diameter/5 from the cell's center of mass and using parameters of ε = 2, N = 100.

The distance between the center of the septum points and the coordinates of both the start and end of the Feret's diameter was determined and the larger of the two was taken to be the mother cell diameter and the smaller, the daughter cell diameter.
To find the septum width, the mean absolute perpendicular distance between all the septum localizations and the line bisecting the angle between the center of the septum, and the mother and daughter diameters was doubled.

Plate reader measurements

Plate reader measurements were carried out on a POLARstar Omega microplate reader (BMG LABTECH). To observe the galactose dependent induction of mNG under the pGAL1 promoter in a Δgal2 background, budding yeast cells were grown overnight in 500 µL of synthetic complete media plus 1% w/v raffinose and galactose concentrations ranging from 0 to 0.1% w/v.

The next morning, 200 µL of this culture was added to individual wells in a 96 well clear bottom plate (Greiner bio-one, item 655096). Cellular fluorescence was excited using the 485 nm excitation filter and measured using the 520 nm emission filter.

The optical density of the cells was measured using the absorbance setting at 600 nm. The fluorescence readings were then normalized to the number of cells by dividing the measured cellular fluorescence by the optical density.

Single-molecule tracking analysis

The LIVE-PAINT images were recorded at a frame rate of 50 ms for 2000 frames. The images were first analyzed using Trackpy[37]. Individual puncta corresponding to cofilin clusters were selected by applying a mask size of 7 and a minimum mass of 2000. The puncta were linked into tracks by applying a maximum displacement of 3 pixels/frame, and a memory of 3 frames (i.e. if the puncta were absent in more than 3 frames, then they were no longer linked to those in previous or subsequent frames). Tracks shorter than 20 frames were discarded, and the mean squared displacement (MSD) plot for the remaining tracks were calculated.

Custom-written code in Igor Pro (Wavemetrics) was used to calculate the initial diffusion co-efficient for each track by fitting the first 250 ms of the MSD to a straight line and determining the gradient. The log of the diffusion coefficients determined from fits with an $r^2 > 0.5$ were then used to populate the diffusion coefficient histogram. A custom code was also used to generate the tracking movies, and the track figure (Figure 6B).

Acknowledgments

We thank Diana Tokarska and Fatima Rafiq for assistance with cloning. We thank Adele Marston and Vasso Makrantoni for the yeast strain BY4741. We thank Chris Wood, Ella Thornton, and Rossana Boni for reading the manuscript and offering helpful suggestions. The authors acknowledge support from NIH R01 GM118528; The Yale Integrated Graduate Program in Physical and Engineering Biology; the School of Biological Sciences at the University of Edinburgh; BBSRC EASTBIO Doctoral Training Partnership; the School of Chemistry at the University of Edinburgh; The Euan MacDonald Centre; Dr. Jim Love and UCB Pharma for providing funding for the microscope; and the UK Dementia Research Institute.

Author Contributions

C.O., M.H.H., S.M., and L.R. designed experiments and wrote the manuscript. C.O., Z.G., L.H., O.K., and M.H.H. acquired data. C.O., Z.G., M.H.H., and L.R. analyzed data.

Ethics Declarations

The authors declare no competing interests.

Data Availability

Source data underlying the figures in the main text will be uploaded to Edinburgh DataShare (DOI will be added when the manuscript is in press).

References

1 Hell, S. W. & Wichmann, J. Breaking the diffraction resolution limit by stimulated emission: stimulated-emission-depletion fluorescence microscopy. *Opt. Lett.* **19**, 780-782, doi:10.1364/OL.19.000780 (1994).

2 Betzig, E. *et al.* Imaging Intracellular Fluorescent Proteins at Nanometer Resolution. *Science* **313**, 1642, doi:10.1126/science.1127344 (2006).

3 Bates, M., Huang, B., Dempsey, G. T. & Zhuang, X. Multicolor Super-Resolution Imaging with Photo-Switchable Fluorescent Probes. *Science* **317**, 1749, doi:10.1126/science.1146598 (2007).

4 Henriques, R., Griffiths, C., Hesper Rego, E. & Mhlanga, M. M. PALM and STORM: Unlocking live-cell super-resolution. *Biopolymers* **95**, 322-331, doi:10.1002/bip.21586 (2011).

5 Rust, M. J., Bates, M. & Zhuang, X. Sub-diffraction-limit imaging by stochastic optical reconstruction microscopy (STORM). *Nature Methods* **3**, 793, doi:10.1038/nmeth929

https://www.nature.com/articles/nmeth929 - supplementary-information (2006).

6 Sharonov, A. & Hochstrasser, R. M. Wide-field subdiffraction imaging by accumulated binding of diffusing probes. *Proc Natl Acad Sci U S A* **103**, 18911-18916, doi:10.1073/pnas.0609643104 (2006).

7 Lemmer, P. *et al.* Using conventional fluorescent markers for far-field fluorescence localization nanoscopy allows resolution in the 10-nm range.

Journal of Microscopy **235**, 163-171, doi:10.1111/j.1365-2818.2009.03196.x (2009).

8 Jungmann, R. *et al.* Single-molecule kinetics and super-resolution microscopy by fluorescence imaging of transient binding on DNA origami. *Nano Lett* **10**, 4756-4761, doi:10.1021/nl103427w (2010).

9 Jungmann, R. *et al.* Multiplexed 3D cellular super-resolution imaging with DNA-PAINT and Exchange-PAINT. *Nat Methods* **11**, 313-318, doi:10.1038/nmeth.2835 (2014).

10 Jungmann, R. *et al.* Quantitative super-resolution imaging with qPAINT. *Nat Methods* **13**, 439-442, doi:10.1038/nmeth.3804 (2016).

11 Schnitzbauer, J., Strauss, M. T., Schlichthaerle, T., Schueder, F. & Jungmann, R. Super-resolution microscopy with DNA-PAINT. *Nat Protoc* **12**, 1198-1228, doi:10.1038/nprot.2017.024 (2017).

12 Strauss, S. *et al.* Modified aptamers enable quantitative sub-10-nm cellular DNA-PAINT imaging. *Nat Methods* **15**, 685-688, doi:10.1038/s41592-018-0105-0 (2018).

13 Melak, M., Plessner, M. & Grosse, R. Actin visualization at a glance. *J Cell Sci* **130**, 525-530, doi:10.1242/jcs.189068 (2017).

14 Okreglak, V. & Drubin, D. G. Cofilin recruitment and function during actin-mediated endocytosis dictated by actin nucleotide state. *J Cell Biol* **178**, 1251-1264, doi:10.1083/jcb.200703092 (2007).

15 Speltz, E. B., Nathan, A. & Regan, L. Design of Protein-Peptide Interaction Modules for Assembling Supramolecular Structures in Vivo and in Vitro. *ACS Chem Biol* **10**, 2108-2115, doi:10.1021/acschembio.5b00415 (2015).

16 Jackrel, M. E., Cortajarena, A. L., Liu, T. Y. & Regan, L. Screening Libraries To Identify Proteins with Desired Binding Activities Using a Split-GFP Reassembly Assay. *ACS Chemical Biology* **5**, 553-562, doi:10.1021/cb900272j (2010).

17 Thompson, K. E., Bashor, C. J., Lim, W. A. & Keating, A. E. SYNZIP protein interaction toolbox: in vitro and in vivo specifications of heterospecific coiled-coil interaction domains. *ACS Synth Biol* **1**, 118-129, doi:10.1021/sb200015u (2012).

18 Chen, R. *et al.* A Barcoding Strategy Enabling Higher-Throughput Library Screening by Microscopy. *ACS Synthetic Biology* **4**, 1205-1216, doi:10.1021/acssynbio.5b00060 (2015).

19 Gavrikov, A. S., Baranov, M. S. & Mishin, A. S. Live-cell nanoscopy with spontaneous blinking of conventional green fluorescent proteins. *Biochemical and Biophysical Research Communications* **522**, 852-854, doi:https://doi.org/10.1016/j.bbrc.2019.11.163 (2020).

20 Shaner, N. C. *et al.* A bright monomeric green fluorescent protein derived from Branchiostoma lanceolatum. *Nat Methods* **10**, 407-409, doi:10.1038/nmeth.2413 (2013).

21 Karasawa, S., Araki, T., Nagai, T., Mizuno, H. & Miyawaki, A. Cyan-emitting and orange-emitting fluorescent proteins as a donor/acceptor pair for fluorescence resonance energy transfer. *Biochemical Journal* **381**, 307-312, doi:10.1042/BJ20040321 (2004).

22 Shaner, N. C. *et al.* Improved monomeric red, orange and yellow fluorescent proteins derived from Discosoma sp. red fluorescent protein. *Nat Biotechnol* **22**, 1567-1572, doi:10.1038/nbt1037 (2004).

23 Hinrichsen, M. *et al.* A new method for post-translationally labeling proteins in live cells for fluorescence imaging and tracking. *Protein Eng Des Sel* **30**, 771-780, doi:10.1093/protein/gzx059 (2017).

24 Hawkins, K. M. & Smolke, C. D. The regulatory roles of the galactose permease and kinase in the induction response of the GAL network in Saccharomyces cerevisiae. *J Biol Chem* **281**, 13485-13492, doi:10.1074/jbc.M512317200 (2006).

25 Courtemanche, N., Pollard, T. D. & Chen, Q. Avoiding artefacts when counting polymerized actin in live cells with LifeAct fused to fluorescent proteins. *Nat Cell Biol* **18**, 676-683, doi:10.1038/ncb3351 (2016).

26 Nagasaki, A. *et al.* The Position of the GFP Tag on Actin Affects the Filament Formation in Mammalian Cells. *Cell Structure and Function* **42**, 131-140, doi:10.1247/csf.17016 (2017).

27 Mund, M. *et al.* Systematic Nanoscale Analysis of Endocytosis Links Efficient Vesicle Formation to Patterned Actin Nucleation. *Cell* **174**, 884-896 e817, doi:10.1016/j.cell.2018.06.032 (2018).

28 Chen, Q., Nag, S. & Pollard, T. D. Formins filter modified actin subunits during processive elongation. *J Struct Biol* **177**, 32-39, doi:10.1016/j.jsb.2011.10.005 (2012).

29 Perfilov, M. M. *et al.* Highly photostable fluorescent labeling of proteins in live cells using exchangeable coiled coils heterodimerization. *Cellular and Molecular Life Sciences*, doi:10.1007/s00018-019-03426-5 (2020).

30 Wäldchen, S., Lehmann, J., Klein, T., van de Linde, S. & Sauer, M. Light-induced cell damage in live-cell super-resolution microscopy. *Scientific Reports* **5**, 15348, doi:10.1038/srep15348 (2015).

31 Bozhanova, N. G. *et al.* Protein labeling for live cell fluorescence microscopy with a highly photostable renewable signal. *Chemical Science* **8**, 7138-7142, doi:10.1039/C7SC01628J (2017).

32 Gwosch, K. C. *et al.* MINFLUX nanoscopy delivers 3D multicolor nanometer resolution in cells. *Nature Methods*, doi:10.1038/s41592-019-0688-0 (2020).

33 Thomas, F., Boyle, A. L., Burton, A. J. & Woolfson, D. N. A set of de novo designed parallel heterodimeric coiled coils with quantified dissociation constants in the micromolar to sub-nanomolar regime. *J Am Chem Soc* **135**, 5161-5166, doi:10.1021/ja312310g (2013).

34 Guthrie, C. & Fink, G. R. *Guide to yeast genetics and molecular and cell biology. Part C Part C*. (Academic Press, 2002).

35 Sander, J., Ester, M., Kriegel, H.-P. & Xu, X. Density-Based Clustering in Spatial Databases: The Algorithm GDBSCAN and Its Applications. *Data Mining and Knowledge Discovery* **2**, 169-194, doi:10.1023/A:1009745219419 (1998).

36 Gould, T. J., Verkhusha, V. V. & Hess, S. T. Imaging biological structures with fluorescence photoactivation localization microscopy. *Nature Protocols* **4**, 291-308, doi:10.1038/nprot.2008.246 (2009).

37 trackpy: Trackpy v0.4.1 (Zenodo, 2018).